Strain-assisted topochemical synthesis of La-doped $SrVO_2H$ films

Hiroshi Takatsu,[*,†,‡] Masayuki Ochi,[¶] Morito Namba,[†] Haobo Li,[†] Aurelien Daniel,[†,§] Takahito Terashima,[‖] Kazuhiko Kuroki,[¶] and Hiroshi Kageyama[*,†]

†*Department of Energy and Hydrocarbon Chemistry, Graduate School of Engineering, Kyoto University, Kyoto 615-8510, Japan*

‡*Engineering Education Research Center, Graduate School of Engineering, Kyoto University, Kyoto 615-8510, Japan*

¶*Department of Physics, Osaka University, Machikaneyama-cho, Toyonaka, Osaka 560-0043, Japan*

§*École Supérieure d'Ingénieurs de Rennes (ESIR), Université de Rennes 1, Campus de Beaulieu, 263, Avenue du Général Leclerc, 35042 Rennes CEDEX, France*

‖*Department of Physics, Graduate School of Science, Kyoto University, Kyoto 606-8502, Japan*

E-mail: takatsu@scl.kyoto-u.ac.jp; kage@scl.kyoto-u.ac.jp

Abstract

Perovskite oxyhydride $SrVO_2H$ (V^{3+}, d^2) is a Mott insulator with a two-dimensional strong correlation due to anion ordering. In this study, we attempted electron doping by aliovalent substitution. Although $Sr_{1-x}La_xVO_3$ thin films ($x \leq 0.4$) on a $SrTiO_3$ substrate were topochemically reduced using CaH_2, the vanadium valence of the reduced films retained trivalent. Combined with the result of secondary ion

mass spectroscopy, we conclude that $Sr_{1-x}La_xVO_{2+x}H_{1-x}$ is obtained, where the apical oxygen site is partially replaced by the hydride anion. First-principles theoretical calculations highlight the role played by compressive biaxial strain in stabilizing the charge-compensated $Sr_{1-x}La_xVO_{2+x}H_{1-x}$ phase, rather than the electron-doped $Sr_{1-x}La_xVO_2H$. The present study demonstrates that topochemical reactions combined with substrate strain provide various opportunities to widen a compositional space in mixed-anion compounds.

Introduction

The oxyhydride $SrVO_2H$ is an anion-ordered perovskite, where hydride anions (H^-) completely occupy the apical site and thus is related to the infinite layer structure $SrCuO_2$, the simplest parent compound among cupric high–T_c superconductors (Figure 1a).[1–5] While order-disorder of anions in mixed-anion compounds is an important topic and challenge,[6] $SrVO_2H$ offers a prototypical example of anion order, where the d–electron count (i.e., d^2) is responsible for the ordered arrangement of *trans*–VO_4H_2 octahedra (Figure 1b).[1,7] Moreover, strong electron correlation causes the half–filled d_{xz}/d_{yz} bands to split, and $SrVO_2H$ becomes a quasi–two–dimensional (2D) Mott insulator.[1,4]

A few attempts have been made to control the Mott insulating state of $SrVO_2H$.[8,9] One example is the application of high pressure,[8] which results in an insulator–to–metal transition at $\sim$ 50 GPa. The quasi 2D nature in both insulating and metallic states is due to the orthogonal $V_{d\pi}$–H_{1s}–$V_{d\pi}$ arrangement.[8] The other example is the chemical substitution of V (B-site) with Ti, corresponding to a filling control.[9] The Ti doping ($\sim$5%), however, results in the loss of anion order and changes the original tetragonal symmetry to cubic, while receiving an excess amount of H^- to give $SrVO_{1.5}H_{1.5}$.

This study reports on the aliovalent Sr (A-site) substitution in order to dope electrons to the half-filled Mott insulator. We examined a CaH_2 topochemical reduction of $Sr_{1-x}La_xVO_3$ both in powder and epitaxial thin film forms, and found that only the latter can be anion-

exchanged. However, it is unexpectedly observed that the V^{3+} state of $Sr_{1-x}La_xVO_3$ after hydride reduction remains unchanged. Secondary ion mass spectroscopy (SIMS) indicated the composition of $Sr_{1-x}La_xVO_{2+x}H_{1-x}$ where the La substitution is compensated by a partial anion exchange. Using first principles calculations, we discuss the origin of the charge compensation and the role of biaxial strain from the substrate for the synthesis of $Sr_{1-x}La_xVO_{2+x}H_{1-x}$.

Experiments and calculations

Polycrystalline samples of $Sr_{1-x}La_xVO_3$ ($x = 0.1, 0.2, 0.3, 0.4$) were prepared using high-temperature solid state reactions from the stoichiometric mixture of $SrCO_3$, V_2O_5, and La_2O_3 at 1350 °C in an H_2/Ar mixed gas flow (H_2 2%), following the literature.[10] Several intermediate grindings were carried out to ensure the completion of the reaction. These La-substituted powder samples were used for topochemical reactions with CaH_2 and as targets for thin film growth. For the former purpose, we used the same method as described in Refs. 1 and 9. That is, a mixture of about 0.6 g of $Sr_{1-x}La_xVO_3$ powder and about 0.2 g of CaH_2 powder was pelletized, vacuum-sealed in a quartz tube, and then heated multiple times at 550 – 600 °C for 2 days. After the reaction, the products were washed with a 0.1M NH_4Cl/methanol solution.

Epitaxial thin films of $Sr_{1-x}La_xVO_3$ precursors with a thickness of 15 – 60 nm were grown on (001)-oriented $SrTiO_3$ (STO) substrates using pulsed laser deposition (PLD). $Sr_{1-x}La_xVO_3$ powder specimens ($x = 0.1, 0.2, 0.3, 0.4$) were used for the epitaxial growth, except for $x = 0$ where $Sr_2V_2O_7$ was used, prepared by standard solid-state reaction at 800 °C in air. The films were deposited at a substrate temperature of 700 – 750 °C under vacuum ($\sim 1 \times 10^{-6}$ Pa), using a KrF excimer laser ($\lambda = 248$ nm) with an energy density of 0.6 J/cm^2 and a repetition rate of 1 Hz. Subsequently, the as-grown film was embedded together with 0.2 g of CaH_2 powder in an evacuated quartz tube, and then heated at 550 °C

for 4 days, followed by washing with 0.1 M NH_4Cl/methanol as in the case of the powder. The shorter diffusion length of the anions required for thin film samples allows for lower reaction temperatures than for powder samples.[1,9]

X-ray diffraction (XRD) measurements were conducted at room temperature (RT) using a Rigaku SmartLab diffractometer with a Cu Kα radiation. The valence state was estimated by the X-ray absorption near-edge structure (XANES) spectroscopy at the V K edge and X-ray photoelectron spectroscopy (XPS). XANES spectra of $Sr_{1-x}La_xVO_3$ thin films after hydride reaction, $SrVO_3$, and $EuVO_3$ were collected at RT on the BL01B1 beamline at SPring-8. Here, $SrVO_3$ and $EuVO_3$ were used as references of V^{4+} and V^{3+}, respectively.[4,11] We reconfirmed Eu^{3+} (thus V^{3+}) in $EuVO_3$ by the XANES spectrum near the Eu L_3 edge. For the XANES measurements, the incident X-ray beam was monochromatized by a Si(111) double–crystal monochromator and the spectra were recorded in the fluorescence mode using a 19–element Ge solid-state detector. XPS spectra were collected at RT using ULVAC–PHI MT–5500 ($h\nu$ = 1253.6 eV; Mg Kα radiation). The binding energy (E_B) of each XPS spectrum with potential extrinsic E_B shifts caused by the charging effect was calibrated with the adventitious C 1s peak at 284.5 eV. SIMS measurements were performed using PHI ADEPT1010 at RT to detect and quantify hydrogen in the films. The primary ion of Cs^+ accelerated at 2 keV was used to obtain depth profiles at 81×81 μm^2 areas for each film.

In order to investigate the structural stability, the first–principles calculations were conducted using the projector–augmented–wave method,[12] as implemented in the Vienna *ab* initio simulation package (VASP).[13–16] We used the local–density approximation with the Perdew-Zunger parametrization[17] based on Quantum Monte-Carlo simulations for the homogeneous electron gas by Ceperley and Alder.[18] For V–d orbitals, we included a $+U$correction[19,20] with $U_{\rm eff} = U - J = 6$ eV. Given the G–type antiferromagnetic order known for $SrVO_2H$,[1] the DFT+U calculations incorporated a strong Coulomb repulsion. The following orbitals for each element were treated as core electrons in the pseudopotentials: [Kr] $4d^{10}$ for La, [Ar] $3d^{10}$ for Sr, [Ne] for V and Ca, and [He] for O. The total energy was examined after optimiz-

ing the crystal structure until the Hellmann-Feynman force acting on each atom becomes less than 0.01 eV/A. The total energy of H^2 molecule was evaluated in the 12 Å×12 Å×12 Å cell. The plane-wave cutoff energy was 550 eV.

Result and discussion

Synthesis

Powder XRD diffraction profiles for $Sr_{1-x}La_xVO_3$ precursors ($0 \leq x \leq 0.4$) indicated the target phase formation up to $x = 0.4$ without any impurities (Supporting Information, Figure S1). The lattice parameter a estimated by Le Bail analysis increases linearly as x increases from $x = 0$ ($SrVO_3$),[21,22] consistent with previous reports.[23,24] However, all of the reactions with CaH_2 on powder samples have failed except for $x = 0$, with several impurity phases included. For example, the XRD pattern of $x = 0.1$ after 4 days of reduction showed tetragonal and cubic phases, along with impurity phases such as VO_2 and $LaSrVO_4$ (Figure 2). The cubic phase appears to be slightly reduced $Sr_{0.9}La_{0.1}VO_{3-\delta}$, whereas the lattice parameters of the tetragonal phase, $a = 3.9354(3)$ Å, $c = 3.6740(4)$ Å, are very close to $a = 3.9331(4)$ Å and $c = 3.6771(3)$ Å for $SrVO_2H$.[1] Since this difference in the lattice parameters is of the same order of magnitude as that between $SrVO_3$ (3.8424(2) Å[21,22]) and $Sr_{0.9}La_{0.1}VO_3$ (3.8483(3) Å), we cannot exclude the possibility that $Sr_{0.9}La_{0.1}VO_2H$ is only partially produced. However, this tetragonal phase completely disappeared in the 10–day (2 days × 5) reaction. Note that in $SrV_{0.95}Ti_{0.05}O_3$, increasing the reaction time with CaH_2 results in cubic $SrV_{0.95}Ti_{0.05}O_{1.5}H_{1.5}$.[9]

The failure of the topochemical reduction of powder led us to use single–crystal films since metastable materials are often stabilized under biaxial substrate strain.[25–27] Precursors of $Sr_{1-x}La_xVO_3$ ($x \leq 0.4$) epitaxial thin films were synthesized on the (001)-STO substrate, showing the excellent orientation along the c axis (Supporting Information, Figure S2). Figure 3 shows out–of–plane $\theta - 2\theta$ XRD patterns of $Sr_{1-x}La_xVO_3$ films ($x = 0.0, 0.2, 0.4$) before

and after the reaction with CaH_2. The $x = 0$ precursor shows a peak at 47.7°(corresponding to the 002 reflection), while it shifts to 49.4° after the reaction (Figure 3a) in consistent with the previous result of $SrVO_2H$ films on STO.[4] The lattice parameter after the reaction is $c = 3.68$ Å. A similar peak shift is observed with increasing x (Figure 3b), but only slightly for $x = 0.4$ (Figure 3c).

In Figure 4a we show the $\theta - 2\theta$ XRD results of the samples after the reaction with CaH_2. With increasing x, a systematic shift of the 002 peak toward the lower angle is observed, suggesting a continuous expansion of the c axis by La doping. There was no sign of impurity phases. The reciprocal space mappings (RSM) around the 103 reflection (Figures 4b–f) shows that the q_x values corresponding to the 103 peak are located in the vicinity of that of the STO substrate, indicating that the film grows coherently, i.e., under the biaxial strain from the STO substrate. Other reflections such as 101, 112, and 213 (not shown) are also compatible with the tetragonal symmetry. These facts suggest that unlike powder samples, the thin film samples are converted topochemically to the $SrVO_2H$–type structure by the hydride reduction combined with the biaxial substrate strain. The substrate employed appears critical for hydride introduction since when a $(La_{0.3}Sr_{0.7})(Al_{0.65}Ta_{0.35})O_3$ (LSAT) substrate is used for $x = 0$, an oxygen-depleted phase results.[4,28]

As can be seen in Figure 4d, the evolution of the cell parameters as a function of x is highly anisotropic, i.e., a is nearly unchanged while c increases linearly. It is remarkable that the volume change in the oxyhydride films with x is much steeper than that of the parent $Sr_{1-x}La_xVO_3$ solid solution (Figure 4h). If the target phase of $Sr_{1-x}La_xVO_2H$ is formed, one may naively expect the x evolution of the volume to be similar to that of $Sr_{1-x}La_xVO_3$, since the La substitution (x) corresponds to the same amount of electron injection in each series.

Chemical compositions

Figures 5a–c show SIMS depth profiles of H, V, La, O ions in the oxyhydride films at $x = 0$, 0.2, and 0.4. A large amount of hydrogen is observed in all films and the uniform distribution of hydrogen and La is evident from the constant intensity along the depth direction of the film region. Compared to $x = 0$, the change of the depth profile of elements is slower in La-doped films, which could be due to the surface roughness of films because the depth profile of the Ti ion, plotted also in Figure 5, is almost independent of x. Figure 5d shows the ratio of $^1H/^{16}O$ secondary ion intensities, where the values of $^1H/^{16}O$ represent the relative change due to the lack of available standards. One can see that the $^1H/^{16}O$ ratio decreases with increasing x, meaning that the hydrogen content decreases with La substitution. Thus, the composition of the films is likely to be $Sr_{1-x}La_xVO_{3-y}H_y$, not $Sr_{1-x}La_xVO_2H$.

To clarify the composition of the oxyhydride films, XANES and XPS measurements were carried out. Figure 5a shows the V K–edge XANES spectra of these films, along with $SrVO_3$ and $EuVO_3$ as references for V^{4+} and V^{3+}, respectively.[4,11] Importantly, the absorption edge position of V K–edge of all the films is close to that of $EuV^{III}O_3$, indicating the trivalent vanadium state for all the hydride films. The invariant vanadium valence by La substitution is also confirmed by the V $2p$ core-level XPS measurements (Figures 6b,c), where $2p_{3/2}$ ($2p_{1/2}$) peaks are observed at 516 eV (523 eV) for all the hydride films. This result is in contrast to $Sr_{1-x}La_xVO_3$ precursor films, where a shift of the $2p_{3/2}$ ($2p_{1/2}$) peak toward the lower energy is observed with increasing La concentration, meaning electron doping to $SrVO_3$ (Supporting Information, Figure S3). These results, together with the SIMS experiment, indicate that the chemical composition of the oxyhydride films obtained by the present hydride reaction is $Sr_{1-x}La_xVO_{2+x}H_{1-x}$ with an unchanged V^{3+} valence.

In $SrVO_2H$, the highly compressible H^- ions[6] allow to shorten the Sr–O distance and relax the otherwise underbonded Sr^{2+} state, which leads to a large contraction of the c axis.[7] The significant expansion of the c axis (Figure 4g) observed in $Sr_{1-x}La_xVO_{2+x}H_{1-x}$ thin films is reasonable since the apical site is partially occupied by less compressible O^{2-} ions. In

the $Sr_{1-x}La_xVO_{2+x}H_{1-x}$ films ($x \leq 0.4$), the tetragonal structure with the relationship of $c < a(= b)$ is maintained (Figure 4g), ensuring that H^- ions are preferentially occupied at the apical site. However, simply extrapolating the lattice constants results in a cubic crystal structure at about $x = 0.5$, suggesting that at least small H/O anti-site disorder is present in close to this solid solution. In relation to this, we have recently observed that in the transient phase of $SrVO_2H$ under tensile strain, some of the H^- ions are at the equatorial site.[28]

Role of biaxial substrate strain for the O/H exchange in the La-doped $SrVO_2H$

As shown above, hydride reduction of $Sr_{1-x}La_xVO_3$ is only successful in thin films under biaxial substrate strain, and $Sr_{1-x}La_xVO_{2+x}H_{1-x}$ is obtained with the invariant valence of V^{3+}. Although the result is different from our initial motivation, the successful topochemical synthesis of the La-doped solid solution (albeit with extra oxygen) is remarkable given the fact that the $SrVO_2H$ structure has been known as a line phase.[1,9] Recalling that the anion-ordered structure of $SrVO_2H$ (V^{3+}, d^2) is stabilized by filling two electrons into the low-lying d_{xz}/d_{yz} orbitals in the *trans*–VO_4H_2 octahedra,[1] if divalent V^{2+} ions are present, electrons will be doped into the unoccupied d_{xy} orbital, resulting in the destabilization of the *trans*–geometry. Interestingly, a partial occupation of the oxygen at the apical site is seen in lanthanoid–substituted $SrFeO_2$, with a similar c-axis expansion.[29] In this case, the strong covalency in $Fe^{II}O_4$ square-planar coordination accounts for the $Sr_{1-x}Ln_xFeO_{2+x/2}$ composition obtained from $Sr_{1-x}Ln_xFeO_{3-\delta}$, where Ln is a lanthanide ion.

Although our original goal of doping electrons into $SrVO_2H$ is not accomplished, the co-doped charge–compensated $Sr_{1-x}La_xVO_{2+x}H_{1-x}$ shows a dimensional crossover in magnetic interactions. The H^- ion in the SrH layer of $SrVO_2H$ does not have π–symmetry to interact with the V d_{xz}/d_{yz} orbitals, which makes the VO_2 layer magnetically two-dimensional.[8] When H^- at the apical position is replaced partially by O^{2-}, the $V_{d\pi}$–O_{2p}–$V_{d\pi}$ interaction

along the c axis is added. Therefore, a dimensional crossover from 2D to 3D is expected to occur in $Sr_{1-x}La_xVO_{2+x}H_{1-x}$ with increasing x.

In order to theoretically investigate the effects of the O/H exchange in La-doped $SrVO_2H$ and the role of the biaxial strain from the substrate, first–principles calculations were performed. For this purpose, we calculated the total energies of $Sr_{1-x}La_xVO_{2+x}H_{1-x}$ and $Sr_{1-x}La_xVO_2H$ under biaxial strain and estimated the energy difference ΔE before and after the reducing reaction of "$Sr_{1-x}La_xVO_{2+x}H_{1-x} + xCaH_2 \rightarrow Sr_{1-x}La_xVO_2H + xCaO + x/2H_2$". To simplify the calculation, we used a deficient hydrogen content $x = 1/64$ ($\sim$ 1.6%) less than the experimental minimum, where ΔE is given by $E(LaSr_{63}V_{64}O_{129}H_{63}) - E(LaSr_{63}V_{64}O_{128}H_{64}) - E(CaH_2) + E(CaO) + 0.5E(H_2)$. The H^- ion was assumed to be located only at the apical site of the VO_4H_2 (or VO_5H) octahedron. The negative value of ΔE means that the oxide occupation at the apical site is favored. Note that to apply the biaxial strain computationally, the in-plane lattice parameters were fixed to the substrate lattice parameter a_0 (i.e., $a = b = a_0$, $\alpha = \beta = \gamma = 90°$), while other structural parameters were optimized. A similar approach for the estimation of the total energy under biaxial substrate strain has been used in the previous study.[30]

Figure 7 shows calculated results of ΔE via the substrate strain $\Delta a(= (a_0 - a)/a_0)$, estimated from a of bulk $SrVO_2H$.[1] When compressive strain is applied, ΔE shows the negative value, suggesting that $LaSr_{63}V_{64}O_{129}H_{63}$ ($La_{0.016}Sr_{0.984}VO_{2.016}H_{0.984}$) becomes more stable than fully anion-ordered $LaSr_{63}V_{64}O_{128}H_{64}$ ($La_{0.016}Sr_{0.984}VO_2H$). This result is compatible with the experimental result since the STO substrate gives compressive strain ($\Delta a < -0.7\%$). Conversely, this result suggests that the tensile strain of about 1% may be favorable for the growth of $LaSr_{63}V_{64}O_{128}H_{64}$ ($La_{0.016}Sr_{0.984}VO_2H$). However, since the energy dependence of the electron-doped $La_{0.016}Sr_{0.984}VO_2H$ is parabolic (not shown), it is possible that the electron-doped $Sr_{1-x}La_xVO_2H$ phase is destabilized by applying a larger tensile strain. From these results, we can conclude that the compressive strain tends to induce the partial occupation of O^{2-} at the apical site of La–doped $SrVO_2H$, stabilizing $Sr_{1-x}La_xVO_{2+x}H_{1-x}$ rather

than $Sr_{1-x}La_xVO_2H$. Note that when the compressive strain is too large, the total energy of $Sr_{1-x}La_xVO_{2+x}H_{1-x}$ becomes much larger (Supporting Information, Figure S4). This may explain why $Sr_{1-x}La_xVO_{2+x}H_{1-x}$ could not be synthesized on the LSAT substrate that can provide a larger compressive strain than STO (Figure S4).

Conclusion

We have studied the aliovalent La^{3+} substitution for the quasi–2D Mott insulator $SrVO_2H$ (V^{3+}, d^2) for electron doping. The hydride reaction of $Sr_{1-x}La_xVO_3$ ($0 \leq x \leq 0.4$) involving H^-/O^{2-} exchange is successful only for the thin films on the $SrTiO_3$ substrate under compressive strain. However, the trivalent state of vanadium (V^{3+}) is unexpectedly preserved for all the reduced films and gives a $Sr_{1-x}La_xVO_{2+x}H_{1-x}$ composition, where oxide anions at the apical site is incompletely exchanged. This invariant valence of V^{3+}, i.e., the robustness of d^2 state, suggests that the $S = 1$ Mott insulating state in hydride films $Sr_{1-x}La_xVO_{2+x}H_{1-x}$ is preserved. Theoretical calculations verified the experimental results of the epitaxial stabilization of $Sr_{1-x}La_xVO_{2+x}H_{1-x}$ and the role of substrate strain. Although topochemical reactions have been performed using epitaxially grown thin films,[31–35] little attention seems to have been paid to the effect of substrate strain to stabilize metastable phases that cannot be obtained in bulk, apart from the orientation of crystal axes.[34,36] However, recent studies show the compositional and structural modification of mixed-anion compounds with strain, such as the control of anion-vacancy layers in $SrV(O,N)_{3-d}$.[28,37,38] Together with these studies, this work sheds light on the strain engineering of structures by taking an advantage of topochemical reactions assisted by substrate strain, which can significantly change the energy landscape of precursor oxides and lead to novel compounds using topochemical anion-exchange reactions.

Associated content

Supporting Information Available

Additional information on results of powder X-ray diffraction and X-ray photoelectron spectroscopy measurements of $Sr_{1-x}La_xVO_3$ precursors, and the calculated total energy of $Sr_{1-x}La_xVO_{2+x}H_{1-x}$.

Acknowledgement

This work was supported by CREST (JPMJCR142, JPMJCR20R2) and JSPS KAKENHI Grants No.16H06438, No.17H04849, No.17H05481, No.18K13470, No.19H04697, JP19H05058, No.20H00384, and No.21K05227, Toyota Riken Scholar, Research Foundation for the Electrotechnology of Chubu, the Kyoto Technoscience Center, and Ube Industries Foundation. Part of the numerical calculations were performed using the large-scale computer systems provided by the following institutions: the supercomputer center of the Institute for Solid State Physics, the University of Tokyo, the Information Technology Center, the University of Tokyo, and the Cybermedia Center, Osaka University. Computational resources from the Cybermedia Center were provided through the HPCI System Research Project (Project ID hp200007).

References

(1) Romero, F. D.; Leach, A.; Mcller, J. S.; Foronda, F.; Blundell, S. J.; Hayward, M. A. Strontium Vanadium Oxide.Hydrides: "Square-Planar" Two-Electron Phases. *Angew Chem.* **2014**, *126*, 7686.

(2) Wei, Y.; Gui, H.; Li, X.; Zhao, Z.; Zhao, Y.-H.; Xie, W. The effect of hydrogen ordering

on the electronic and magnetic properties of the strontium vanadium oxyhydride. *J. Phys.: Condens. Matter* **2015**, *27*, 206001.

(3) Liu, K.; Hou, Y.; Gong, X.; Xiang, H. Orbital Delocalization and Enhancement of Magnetic Interactions in Perovskite Oxyhydrides. *Sci. Rep.* **2016**, *6*, 19653.

(4) Katayama, T.; Chikamatsu, A.; Yamada, K.; Shigematsu, K.; Tomoya Onozuka, M. M.; Hiroshi Kumigashira, E. I.; Hasegawa, T. Epitaxial growth and electronic structure of oxyhydride $SrVO_2H$ thin films. *J. Appl. Phys.* **2016**, *120*, 085305.

(5) Ochi, M.; Kuroki, K. Effective interaction for vanadium oxyhydrides $Sr_{n+1}V_nO_{2n+1}H_n$ ($n = 1$ and $n \to \infty$): A constrained-RPA study. *Phys. Rev. B* **2019**, *99*, 155143.

(6) Kageyama, H.; Hayashi, K.; Maeda, K.; Attfield, J. P.; Hiroi, Z.; Rondinelli, J. M.; Poeppelmeier, K. R. Expanding frontiers in materials chemistry and physics with multiple anions. *Nat. Commun.* **2018**, *9*, 772.

(7) Ochi, M.; Kuroki, K. Quantifying the stability of the anion ordering in $SrVO_2H$. *Phys. Rev. B* **2020**, *102*, 134108.

(8) Yamamoto, T.; Zeng, D.; Kawakami, T.; Arcisauskaite, V.; Yata, K.; Patino, M. A.; Izumo, N.; McGrady, J. E.; Kageyama, H.; Hayward, M. A. The role of π-blocking hydride ligands in a pressure-induced insulator-to-metal phase transition in $SrVO_2H$. *Nat. Commun.* **2017**, *8*, 1217.

(9) Patino, M. A.; Zeng, D.; Blundell, S. J.; McGrady, J. E.; Hayward, M. A. Extreme Sensitivity of a Topochemical Reaction to Cation Substitution: $SrVO_2H$ versus $SrV_{1-x}Ti_xO_{1.5}H_{1.5}$. *Inorg. Chem.* **2018**, *57*, 2890.

(10) Inaba, F.; Arima, T.; Ishikawa, T.; Katsufuji, T.; Tokura, Y. Change of electronic properties on the doping-induced insulator-metal transition in $La_{1-x}Sr_xVO_3$. *Phys. Rev. B* **1995**, *52*, R2221.

(11) McCarthy, G. J.; Greedan, J. E. Complex Oxides Containing Divalent Europium. I. Guidelines for the Prediction of New Phases. Application to Phases of the Type $EuMO_3$. *Inorg. Chem.* **1975**, *14*, 772.

(12) Kresse, G.; Joubert, D. From ultrasoft pseudopotentials to the projector augmented-wave method. *Phys. Rev. B* **1999**, *59*, 1758.

(13) Kresse, G.; Hafner, J. Ab initio molecular dynamics for liquid metals. *Phys. Rev. B* **1993**, *47*, 558.

(14) Kresse, G.; Hafner, J. Ab initio molecular-dynamics simulation of the liquid-metal amorphous-semiconductor transition in germanium. *Phys. Rev. B* **1994**, *49*, 14251.

(15) Kresse, G.; FurthmMüller, J. Efficiency of ab-initio total energy calculations for metals and semiconductors using a plane-wave basis set. *Comput. Mater. Sci.* **1996**, *6*, 15.

(16) Kresse, G.; FurthmMüller, J. Efficient iterative schemes for ab initio total-energy calculations using a plane-wave basis set. *Phys. Rev. B* **1996**, *54*, 11169.

(17) Perdew, J. P.; Zunger, A. Self-interaction correction to density-functional approximations for many-electron systems. *Phys. Rev. B* **1981**, *23*, 5048.

(18) Ceperley, D. M.; Alder, B. J. Ground State of the Electron Gas by a Stochastic Method. *Phys. Rev. Lett.* **1980**, *45*, 566.

(19) Liechtenstein, A. I.; Anisimov, V. I.; Zaanen, J. Density-functional theory and strong interactions: Orbital ordering in Mott-Hubbard insulators. *Phys. Rev. B* **1995**, *52*, R5467(R).

(20) Dudarev, S. L.; Botton, G. A.; Savrasov, S. Y.; Humphreys, C. J.; Sutton, A. P. Electron-energy-loss spectra and the structural stability of nickel oxide: An LSDA+U study. *Phys. Rev. B* **1998**, *57*, 1505.

(21) Chamberland, B. L.; Danielson, P. S. Alkaline-Earth Vanadium (IV) Oxides Having the AVO$_3$, Composition. *J. Solid State Chem.* **1971**, *3*, 243.

(22) Lan, Y. C.; Chen, X. L.; He, M. Structure, magnetic susceptibility and resistivity properties of SrVO$_3$. *J. Alloys Comp.* **2003**, *354*, 95.

(23) Shin-ike, T.; Sakai, T.; Adachi, C.; Shiokawa, J. Studies on the solid solutions of $Ln_{1-x}Sr_xVO_{3-0.1x}$. *Mat. Res. Bull.* **1976**, *11*, 249.

(24) Mahajan, A. V.; Johnston, D. C.; Torgeson, D. R.; Borsa, F. Structural, electronic, and magnetic properties of $La_xSr_{1-x}VO_3$ ($0.1 \leq x \leq 1.0$). *Phys. Rev. B* **1992**, *46*, 10973.

(25) Gorbenko, O. Y.; Samoilenkov, S. V.; Graboy, I. E.; Kaul, A. R. Epitaxial Stabilization of Oxides in Thin Films. *Chem. Mater* **2002**, *14*, 4026.

(26) Freund, L. B.; Suresh, S. *Thin Film Materials: Stress, Defect Formation and Surface Evolution*; Cambridge University Press: Cambridge, 2003.

(27) Oka, D.; Fukumura, T. Crystal engineering for novel functionalities with oxide thin film epitaxy. *Cryst. Eng. Comm.* **2017**, *19*, 2144.

(28) Namba, M.; Takatsu, H.; Yoshimune, W.; Daniel, A.; Itoh, S.; Terashima, T.; Kageyama, H. A Partial Anion Disorder in SrVO$_2$H Induced by Biaxial Tensile Strain. *Inorganics* **2020**, *8*, 26.

(29) Yamamoto, T.; Ohkubo, H.; Tassel, C.; Hayashi, N.; Kawasaki, S.; Okada, T.; Yagi, T.; Hester, J.; Avdeev, M.; Kobayashi, Y.; ; Kageyama, H. Impact of Lanthanoid Substitution on the Structural and Physical Properties of an Infinite–Layer Iron Oxide. *Inorg. Chem.* **2016**, *55*, 12093.

(30) Takatsu, H.; Ochi, M.; Yamashina, N.; Namba, M.; Kuroki, K.; Terashima, T.; Kageyama, H. Epitaxial Stabilization of $SrCu_3O_4$ with Infinite $Cu_{3/2}O_2$ Layers. *Inorg. Chem.* **2020**, *59*, 10042.

(31) Inoue, S.; Kawai, M.; Ichikawa, N.; Kageyama, H.; Paulus, W.; Shimakawa, Y. Anisotropic oxygen diffusion at low temperature in perovskite-structure iron oxides. *Nat. Chem.* **2010**, *2*, 213.

(32) Kawai, M.; Matsumoto, K.; Ichikawa, N.; Mizumaki, M.; Sakata, O.; Kawamura, N.; Kimura, S.; Shimakawa, Y. Orientation Change of an Infinite-Layer Structure $LaNiO_2$ Epitaxial Thin Film by Annealing with CaH_2. *Cryst. Grwoth Des.* **2010**, *10*, 2044.

(33) Yajima, T.; Kitada, A.; Kobayashi, Y.; Sakaguchi, T.; Bouilly, G.; Kasahara, S.; Takano, T. T. M.; ; Kageyama, H. Epitaxial Thin Films of $ATiO_{3-x}H_x$ (A = Ba, Sr, Ca) with Metallic Conductivity. *J. Am. Chem. Soc.* **2012**, *134*, 8782.

(34) Bouilly, G.; Yajima, T.; Terashima, T.; Kususe, Y.; Fujita, K.; Tassel, C.; Yamamoto, T.; Tanaka, K.; Kobayashia, Y.; Kageyama, H. Substrate-induced anion rearrangement in epitaxial thin films of $LaSrCoO_{4-x}H_x$. *CrystEngComm* **2014**, *16*, 9669.

(35) Katayama, T.; Chikamatsu, A.; Kamisaka, H.; Yokoyama, Y.; Hirata, Y.; Wadati, H.; Fukumura, T.; Hasegawa, T. Topotactic synthesis of strontium cobalt oxyhydride thin film with perovskite structure. *AIP Advances* **2015**, *5*, 107147.

(36) Shimakawa, Y.; Inoue, S.; Haruta, M.; Kawai, M.; Matsumoto, K.; Sakaiguchi, A.; Ichikawa, N.; Isoda, S.; Kurata, H. Topotactic Changes in Thin Films of Brownmillerite $SrFeO_{2.5}$ Grown on $SrTiO_3$ Substrates to Infinite–Layer Structure $SrFeO_2$. *Cryst. Growth Des.* **2010**, *10*, 4713.

(37) Kutsuzawa, D.; Hirose, Y.; Chikamatsu, A.; Nakao, S.; Watahiki, Y.; Harayama, I.; Sekiba, D.; Hasegawa, T. Strain-enhanced topotactic hydrogen substitution for oxygen in $SrTiO_3$ epitaxial thin film. *Appl. Phys. Lett.* **2018**, *113*, 253104.

(38) Yamamoto, T. et al. Strain-induced creation and switching of anion vacancy layers in perovskite oxynitrides. *Nat. Commun.* **2020**, *11*, 5923.

(39) Aritani, H.; Yamada, H.; Yamamoto, T.; Tanaka, T.; Imamura, S. XANES study of Li-MgO and Li-La_2O_3-MgO catalysts for oxidative coupling of methane. *J. Synchrotron Rad.* **2001**, *8*, 593.

(40) Xu, W.; Marcelli, A.; Joseph, B.; Iadecola, A.; Chu, W. S.; Gioacchino, D. D.; Bianconi, A.; Wu, Z. Y.; Saini, N. L. Local structural disorder in REFeAsO oxypnictides by RE L_3 edge XANES. *J. Phys.: Cond. Matter* **2010**, *22*, 125701.

(41) Asakura, H.; Shishido, T.; Teramura, K.; Tanaka, T. Local Structure and La L_1 and L_3-Edge XANES Spectra of Lanthanum Complex Oxides. *Inorg. Chem.* **2014**, *53*, 6048.

...

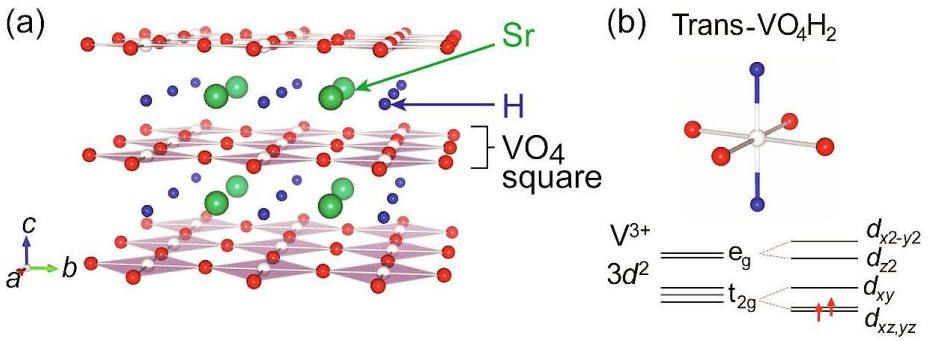

Figure 1: (a) Crystal structure of $SrVO_2H$ (space group $P4/mmm$). (b) local coordination geometry of *trans*-VO_4H_2 (top), and crystal filed splitting of $SrVO_2H$ (bottom). On-site Coulomb interaction further splits the half-filled d_{xz}/d_{yz} band, leading to a Mott insulating ground state in $SrVO_2H$.

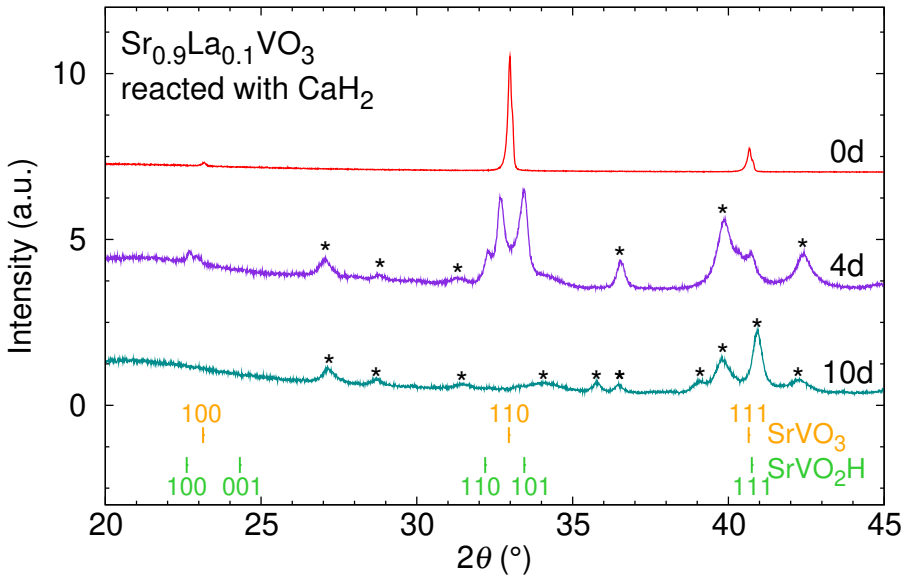

Figure 2: Powder XRD data of $Sr_{0.9}La_{0.1}VO_3$ after the reaction with CaH_2 for 0, and 4 and 10 days. Orange and green lines at the bottom represent the peak positions of $SrVO_3$ and $SrVO_2H$, respectively. Asterisks indicate impurity peaks such as VO_2, V_2O_3, and $LaSrVO_4$, which appeared after reduction. The presence of oxidized impurities in addition to the reduced product is attributed to the partial decomposition of the parent phase.

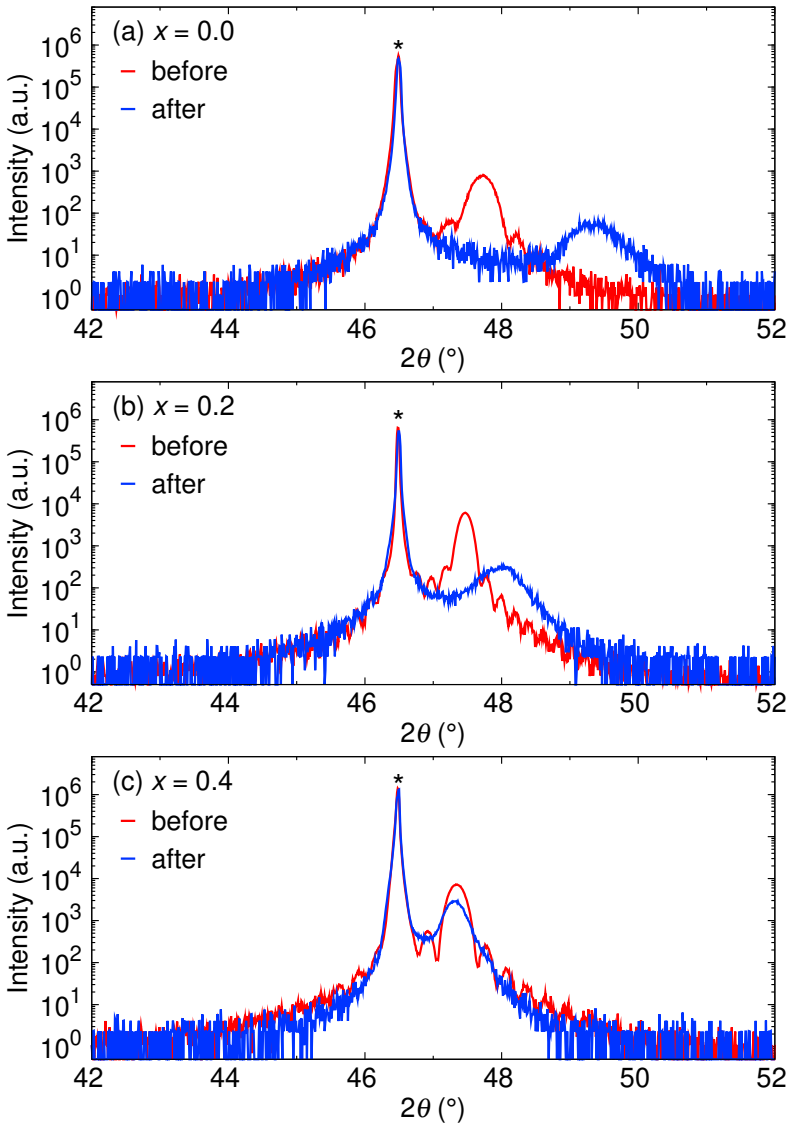

Figure 3: Out–of–plane θ–2θ XRD scans around the 002 peak of $Sr_{1-x}La_xVO_3$ thin films ($x = 0.0, 0.2, 0.4$) before and after the reaction with CaH_2. STO substrate peaks are marked with asterisks.

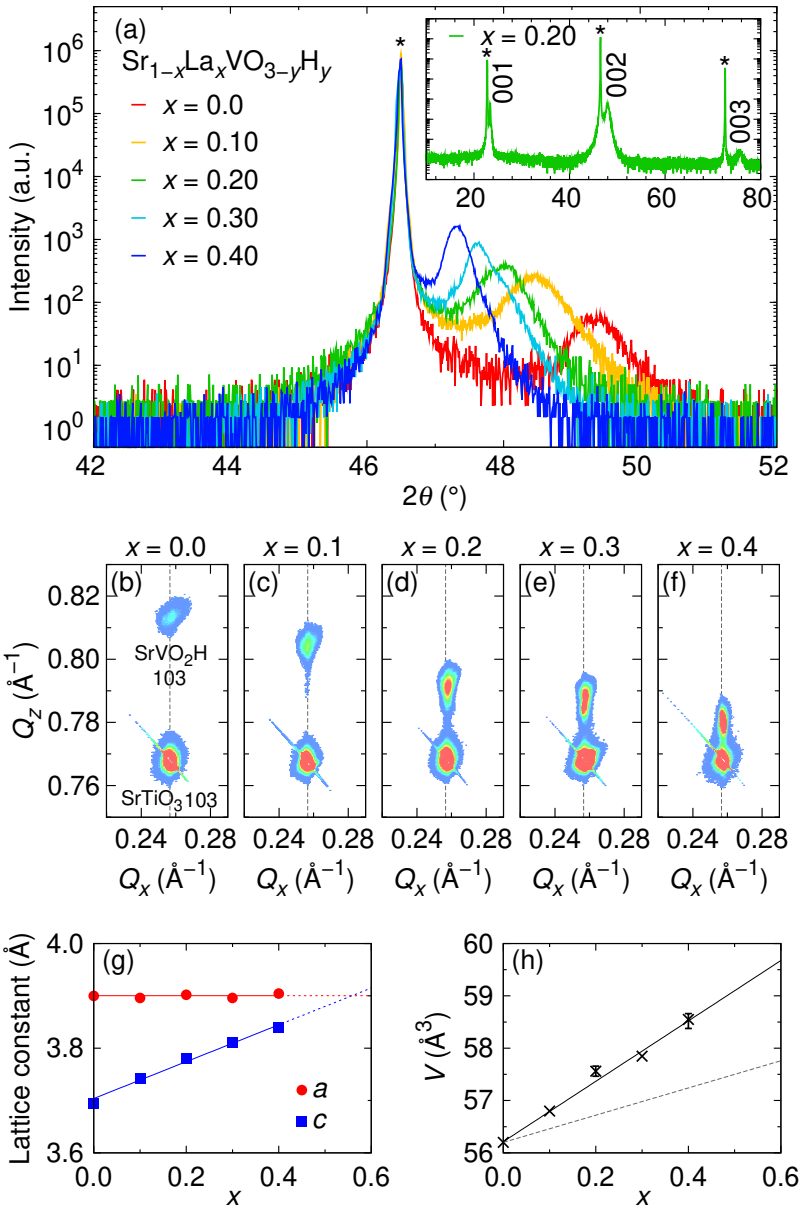

Figure 4: (a) Out–of–plane θ–2θ XRD patterns of $Sr_{1-x}La_xVO_3$ films (x = 0.0, 0.1, 0.2, 0.3, 0.4) on the STO substrate after the reaction with CaH_2, $Sr_{1-x}La_xVO_{3-y}H_y$. The composition of y of H^- content in the samples is discussed in the main text. Inset displays the scan over a wide 2θ rage for the representative of the sample with x = 0.2, showing only $00l$ peaks without any sign of impurity phases. STO substrate peaks are marked with asterisks. (b)-(f) X-ray RSM variations for nominal x, around the 103 reflections of the films and substrate. (g)-(h) The lattice parameters a and c, and volume V, plotted as a function of La content x. The broken line in (h) represents the volume change of the parent oxide $Sr_{1-x}La_xVO_3$.

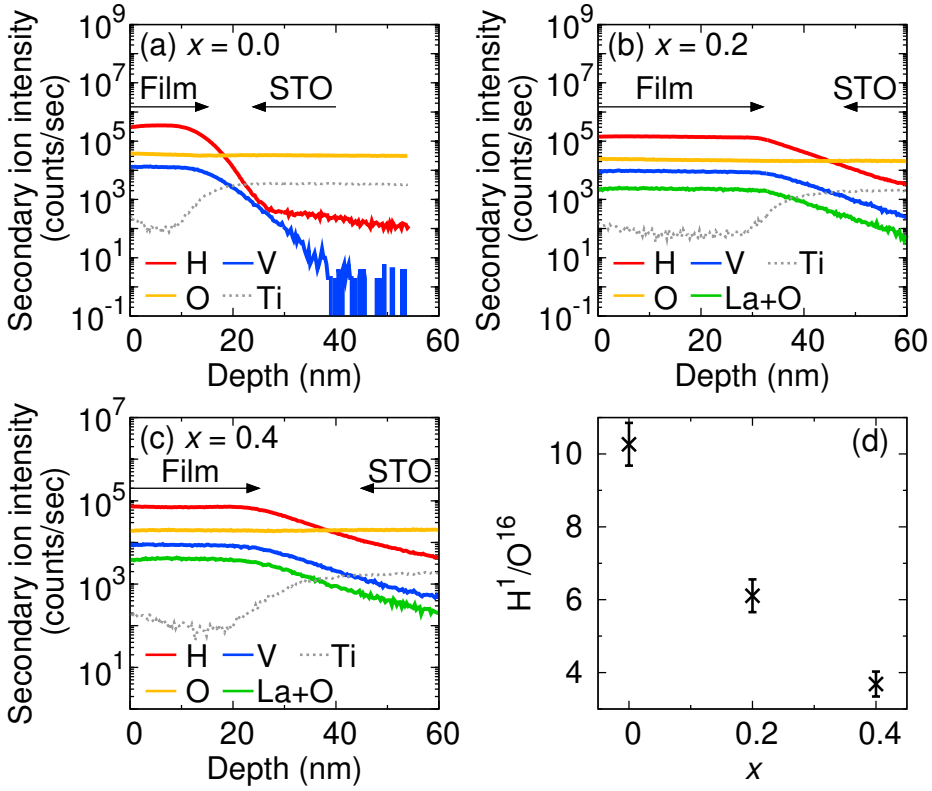

Figure 5: (a)–(c) SIMS depth profiles of $Sr_{1-x}La_xVO_3$ films (x = 0.0, 0.2, 0.4)on the STO substrate, reacted with CaH_2. (d) Secondary ion intensity ratio of $^1H/^{16}O$ in the film region as a function of the nominal La content of x. Note that the values of $^1H/^{16}O$ here represent relative changes because of the lack of available standards.

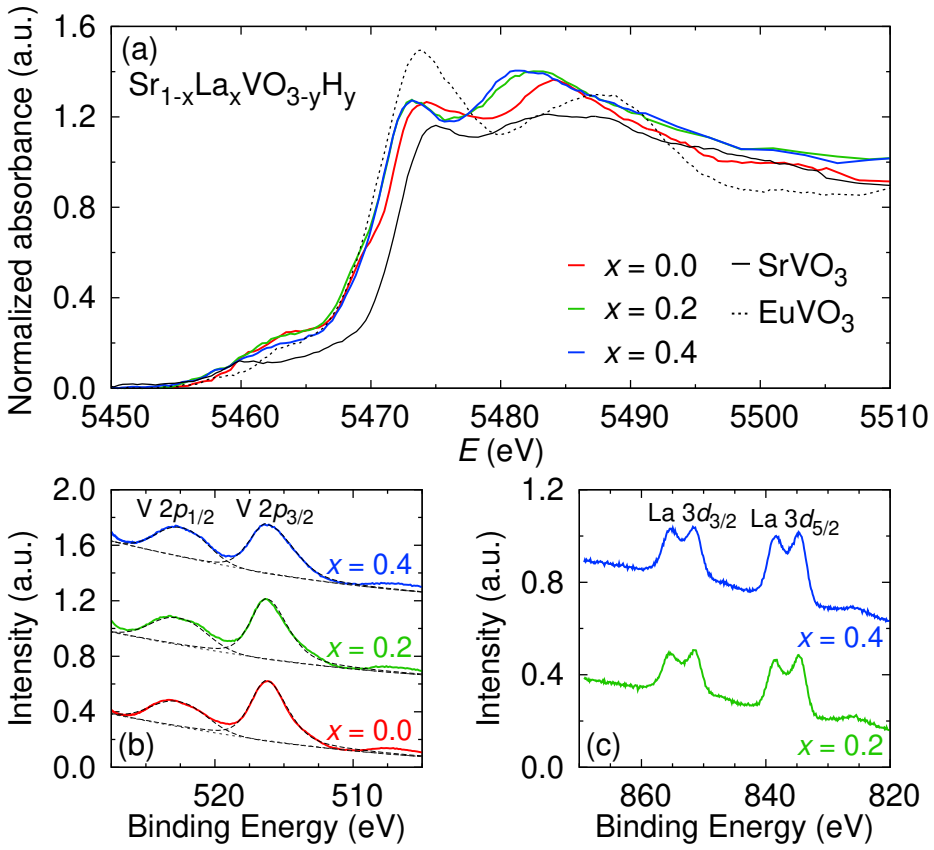

Figure 6: (a) V K-edge XANES spectra of CaH_2-reacted $Sr_{1-x}La_xVO_3$ films (x = 0.0, 0.2, 0.4) and reference samples ($SrVO_3$ and $EuVO_3$). The vanadium valence has been shown to be tetravalent in $SrVO_3$[4] and trivalent in $EuVO_3$.[11] A hump around 5483 eV in the La–doped films may be originated from the strong white line at the La L_3 edge.[39–41] (b) XPS V $2p$ core-level spectra of the films with x = 0.0, 0.2, 0.4. Peak positions are independent on La concentration. Dashed lines represent fits with a single Voigt function for a V $2p_{1/2}$ and $2p_{3/2}$ spectrum, respectively, implying a few distribution of vanadium valence. (c) XPS La $3d$ core-level spectra of La-doped films (x = 0.2, 0.4). The multiplet splitting peaks at $3d_{5/2}$ ($3d_{3/2}$) around 835 eV (852 eV) at the La $3d$ core–level indicate the La^{3+} state.

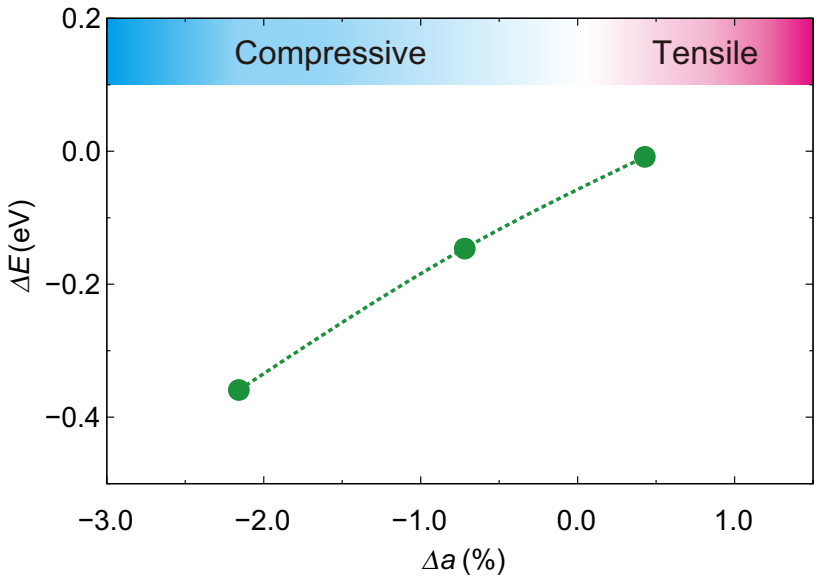

Figure 7: Energy difference $\Delta E = E(\mathrm{LaSr_{63}V_{64}O_{129}H_{63}}) - E(\mathrm{LaSr_{63}V_{64}O_{128}H_{64}}) + E(\mathrm{CaH_2}) - E(\mathrm{CaO}) - 0.5E(\mathrm{H_2})$, plotted as a function of the biaxial strain form the substrate, $\Delta a (= (a_0 - a)/a_0)$, estimated from the in-plane lattice parameter a of bulk $\mathrm{SrVO_2H}$.[1] a_0 is the in-plane lattice parameter of the substrate. The line is the guide to the eye.

TOC graphic and synopsis

"For Table of Contents Use Only"

Strain-assisted topochemical synthesis of La-doped $SrVO_2H$ films

Hiroshi Takatsu, Masayuki Ochi, Morito Namba, Haobo Li, Aurelien Daniel, Takahito Terashima, Kazuhiko Kuroki, and Hiroshi Kageyama

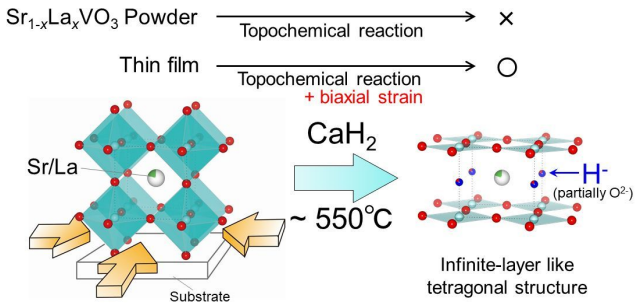

We have succeeded in growing La-doped $SrVO_2H$ under compressive biaxial strain, where the vanadium valence of the reduced films retained trivalent, giving the composition of $Sr_{1-x}La_xVO_{2+x}H_{1-x}$. First principles theoretical calculations showed that the charge compensated phase of $Sr_{1-x}La_xVO_{2+x}H_{1-x}$ is more stable than the electron-doped $Sr_{1-x}La_xVO_2H$ under compressive biaxial strain. The present study demonstrates that topochemical reactions combined with strain engineering open a new avenue for crystal growth and design of complex oxides and mixed-anion compounds.

Supporting Information: Strain-assisted topochemical synthesis of La-doped $SrVO_2H$ films

Hiroshi Takatsu,[*,†,‡] Masayuki Ochi,[¶] Morito Namba,[†] Haobo Li,[†] Aurelien Daniel,[†,§] Takahito Terashima,[‖] Kazuhiko Kuroki,[¶] and Hiroshi Kageyama[*,†]

†*Department of Energy and Hydrocarbon Chemistry, Graduate School of Engineering, Kyoto University, Kyoto 615-8510, Japan*

‡*Engineering Education Research Center, Graduate School of Engineering, Kyoto University, Kyoto 615-8510, Japan*

¶*Department of Physics, Osaka University, Machikaneyama-cho, Toyonaka, Osaka 560-0043, Japan*

§*École Supérieure d'Ingénieurs de Rennes (ESIR), Université de Rennes 1, Campus de Beaulieu, 263, Avenue du Général Leclerc, 35042 Rennes CEDEX, France*

‖*Department of Physics, Graduate School of Science, Kyoto University, Kyoto 606-8502, Japan*

E-mail: takatsu@scl.kyoto-u.ac.jp; kage@scl.kyoto-u.ac.jp

Abstract

In this supporting information, we present powder X-ray diffraction (XRD) data of $Sr_{1-x}La_xVO_3$ polycrystalline precursors (x = 0.1, 0.2, 0.3, 0.4) grown by the high–temperature standard solid–state reaction. We also present the out–of–plane θ–2θ XRD scan data and X-ray photoelectron spectroscopy (XPS) data of $Sr_{1-x}La_xVO_3$

single-crystalline precursor films ($0.0 \leq x \leq 0.4$). The calculated total energy of $Sr_{1-x}La_xVO_{2+x}H_{1-x}$ via the biaxial strain from the substrate is also shown, where the composition with $x = 1/64$ ($\sim 1.6\%$) was examined.

Characterization of $Sr_{1-x}La_xVO_3$ precursors

Polycrystalline samples

Prepared $Sr_{1-x}La_xVO_3$ polycrystalline precursors ($x = 0.1$, 0.2, 0.3, 0.4) were checked by a laboratory X-ray machine at room temperature (RT). The data of all samples show the same XRD pattern of $SrVO_3$,[S1,S2] indicating that the samples crystalize into the cubic structure (space group $Pm\bar{3}m$) in the entire x range synthesized (Figure S1). No traces of impurity peaks and phase segregation were confirmed within the present experimental accuracy. The lattice parameters, estimated by Le Bail analysis, linearly increases with increasing x, which is consistent with previous results[S3,S4] and ensures the successful mixture of the samples in the present study as well.

Single-crystalline thin film samples

Figure S2 shows out–of–plane θ–2θ XRD scans of $Sr_{1-x}La_xVO_3$ single-crystalline thin films ($0.0 \leq x \leq 0.4$) grown on the (001)–oriented $SrTiO_3$ (STO) substrate. The observation of only $00l$ peaks without any sign of impurity phases indicates the excellent orientation of the epitaxial thin films along the c axis. We also confirmed that the $00l$ peaks shift to the lower angle with increasing x, like the polycrystalline samples (Figure S1 and its inset). The slope of the change with respect to x for the c lattice parameter is almost the same as that of the polycrystalline samples (Figure S2 inset), suggesting the formation of the target single-crystalline thin films. A reduction of the c axis in the thin films is due to the biaxial tensile strain from the STO substrate, although it may be also affected by slight oxygen deficiencies. These $Sr_{1-x}La_xVO_3$ precursor thin films were used for the reaction with CaH_2

(see the main text for more details).

Figure S3 shows a V $2p$ core–level XPS spectrum before and after the hydride reaction of the $Sr_{1-x}La_xVO_3$ thin films with CaH_2. Before the reaction, the $2p_{3/2}$ ($2p_{1/2}$) peak systematically shifts toward the lower energy with increasing La contents of x (Figure S3a). On the other hand, the peak shift by La doping is not observed after the reaction of the films with CaH_2 (Figure S3b). The shift observed in the samples before the hydride reaction is about 0.3 and 0.6 eV at $x = 0.2$ and 0.4 from the peak at $x = 0.0$, respectively. Since the energy interval between V^{3+} and V^{4+} is about 1.5 eV,[S5–S7] these shifts agree with what we can simply expect from La doping that gives $\Delta E = 1.5x$. These energy shifts can be reproduced by fitting with the two Voight functions represented by contributions of the V^{3+} and V^{4+} spectra (dashed lines in Figure S3a), where the peak positions of V^{3+} and V^{4+} were fixed at 515 and 516.5 eV, as found in the previous results.[S5–S7] These results well support the formation of $Sr_{1-x}La_xVO_3$ thin films. The XPS results of thin films after the hydride reaction are discussed further in the main text.

Total energy of $Sr_{1-x}La_xVO_{2+x}H_{1-x}$ via biaxial strain

Figure S4 shows the calculated result of the total energy of $Sr_{1-x}La_xVO_{2+x}H_{1-x}$ with $x = 1/64$, plotted as a function of a_0, where the upper axis shows the biaxial substrate strain, $\Delta a (= (a_0 - a)/a_0)$, estimated from the in-plane lattice parameter a of bulk $SrVO_2H$.[S8] Here, a_0 is the substrate lattice parameter. One can see that the total energy takes a minimum around $a_0 = 3.95$ Å, which is close to the lattice parameter of the $SrTiO_3$ (STO) substrate (3.905 Å).[S9] This result suggests that $Sr_{1-x}La_xVO_{2+x}H_{1-x}$ is potentially obtained, stabilized by the biaxial strain from the STO substrate. On the other hand, $Sr_{1-x}La_xVO_{2+x}H_{1-x}$ may not be obtained on a $(La_{0.3}Sr_{0.7})(Al_{0.65}Ta_{0.35})O_3$ (LSAT) substrate, since the total energy around $a_0 = 3.868$ Å, which corresponds to the lattice parameter of LSAT,[S9] is larger than that around 3.95 Å(Figure S4), implying that $Sr_{1-x}La_xVO_{2+x}H_{1-x}$ is unstable for much

larger compressive strain.

References

(S1) Chamberland, B. L.; Danielson, P. S. Alkaline-Earth Vanadium (IV) Oxides Having the AVO$_3$, Composition. *J. Solid State Chem.* **1971**, *3*, 243.

(S2) Lan, Y. C.; Chen, X. L.; He, M. Structure, magnetic susceptibility and resistivity properties of SrVO$_3$. *J. Alloys Comp.* **2003**, *354*, 95.

(S3) Shin-ike, T.; Sakai, T.; Adachi, C.; Shiokawa, J. Studies on the solid solutions of $Ln_{1-x}Sr_xVO_{3-0.1x}$. *Mat. Res. Bull.* **1976**, *11*, 249.

(S4) Mahajan, A. V.; Johnston, D. C.; Torgeson, D. R.; Borsa, F. Structural, electronic, and magnetic properties of $La_xSr_{1-x}VO_3$ ($0.1 \leq x \leq 1.0$). *Phys. Rev. B* **1992**, *46*, 10973.

(S5) Maiti, K.; Manju, U.; Ray, S.; Mahadevan, P.; Inoue, I. H.; Carbone, C.; Sarma, D. D. Understanding the bulk electronic structure of $Ca_{1-x}Sr_xVO_3$. *Phys. Rev. B* **2006**, *73*, 052508.

(S6) Hotta, Y.; Wadati, H.; Fujimori, A.; Susaki, T.; Hwang, H. Y. Electronic structure of the Mott insulator LaVO$_3$ in a quantum well geometry. *Appl. Phys. Lett.* **2006**, *89*, 251916.

(S7) Wadati, H.; Hotta, Y.; Fujimori, A.; Susaki, T.; Hwang, H. Y.; Takata, Y.; Horiba, K.; Matsunami, M.; Shin, S.; Yabashi, M.; Tamasaku, K.; Nishino, Y.; Ishikawa, T. Hard x-ray photoemission study of LaAlO$_3$/LaVO$_3$ multilayers. *Phys. Rev. B* **2008**, *77*, 045122.

(S8) Romero, F. D.; Leach, A.; Mcller, J. S.; Foronda, F.; Blundell, S. J.; Hayward, M. A. Strontium Vanadium Oxide.Hydrides: "Square-Planar" Two-Electron Phases. *Angew Chem.* **2014**, *126*, 7686.

(S9) Schlom, D. G.; Chen, L.-Q.; Fennie, C. J.; Gopalan, V.; Muller, D. A.; Pan, X.; Ramesh, R.; Uecker, R. Elastic strain engineering of ferroic oxides. *MRS Bulletin* **2014**, *39*, 118.

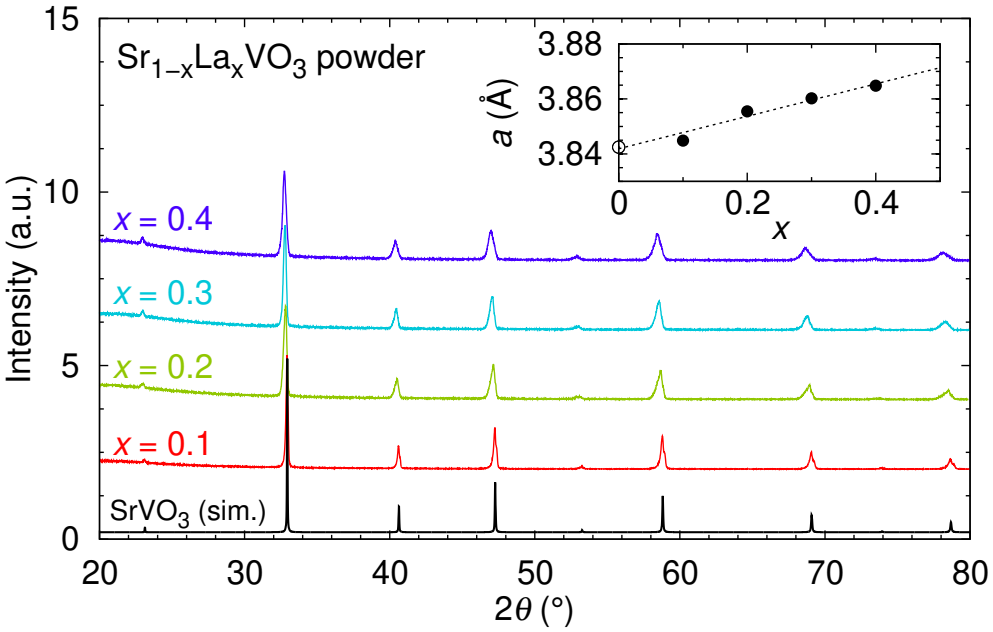

Figure S1: Powder XRD patterns of $Sr_{1-x}La_xVO_3$ polycrystalline precursors ($x = 0.1$, 0.2, 0.3, 0.4) at RT. The data of $SrVO_3$ is a calculated result using structural parameters from Ref. S2. Inset is the lattice parameter a plotted as a function of x. The data for $x = 0.0$ are taken from the previous literatures.[S1,S2]

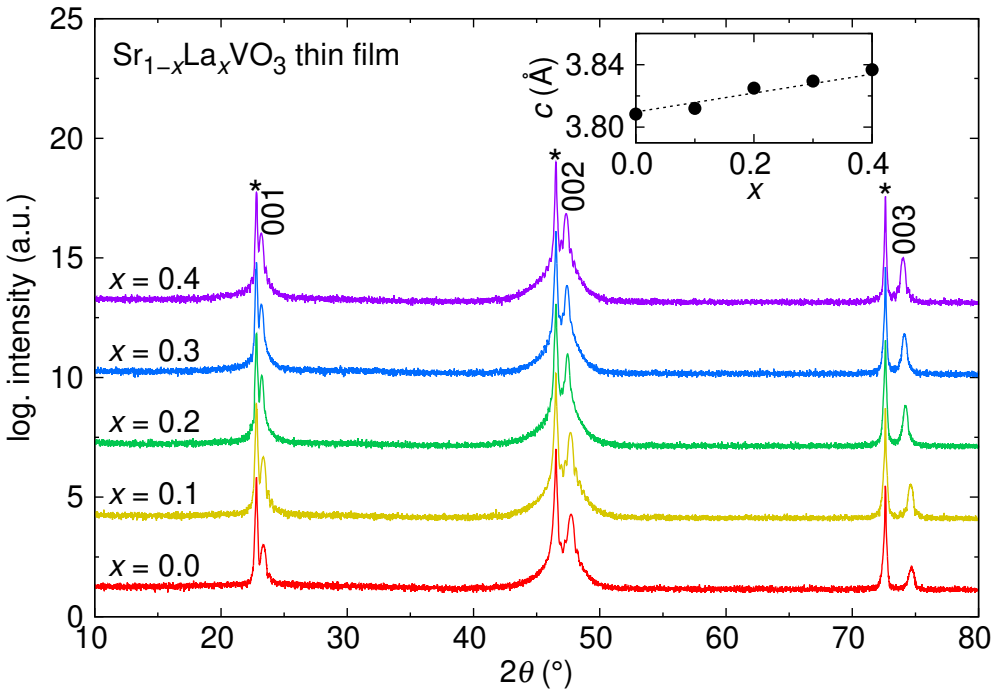

Figure S2: Out–of–plane θ–2θ XRD patterns of single-crystalline $Sr_{1-x}La_xVO_3$ precursor thin films ($0.0 \leq x \leq 0.4$) on the (001)–oriented STO substrate. STO substrate peaks are marked with asterisks. The inset shows the lattice parameter of the c axis, estimated from the 002 peak, as a function of x. The slope of the change with respect to x is almost the same as that of polycrystalline samples (Figure S1 inset). The reduction of the c axis, compared with the polycrystalline samples, is due to the biaxial tensile strain from the STO substrate to precursor thin films of $Sr_{1-x}La_xVO_3$.

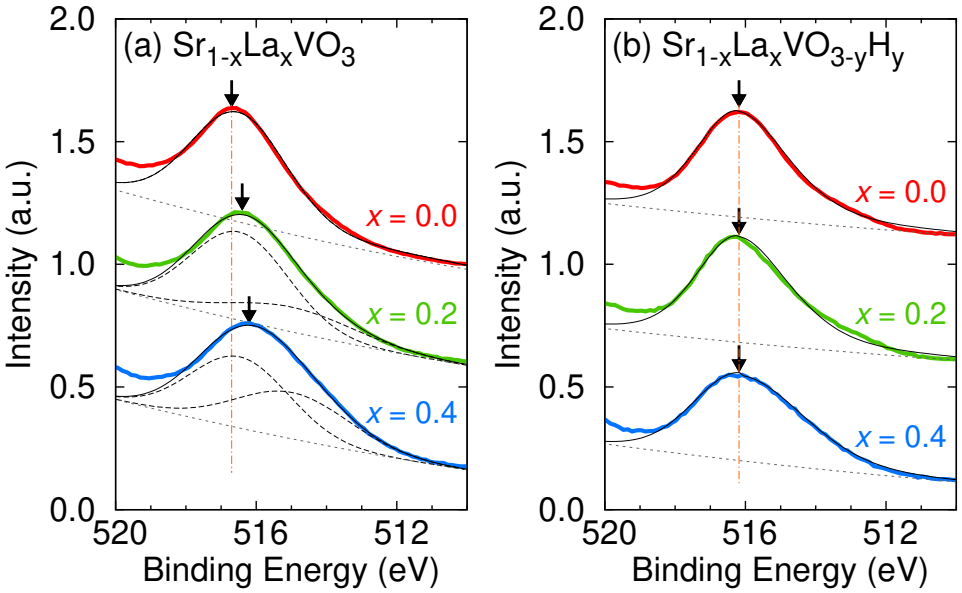

Figure S3: XPS V $2p$ core–level spectra of $Sr_{1-x}La_xVO_3$ thin films ($x = 0.0$, 0.2, 0.4) before and after the reaction with CaH_2. The data are shown near the $2p_{3/2}$ peak. A clear peak shift is observed in precursor films (Figure S3a), while the peak position is independent of films after the reaction (Figure S3b). Solid lines represent fits with Voigt functions, where the spectra of the precursor phase of $x = 0.0$ and the sample after the hydride reaction were fitted with a single function, while the spectra of the precursor $x = 0.2$ and 0.4 samples were fitted by two Voigt functions represented by contributions from the V^{3+} and V^{4+} spectra (dashed lines).

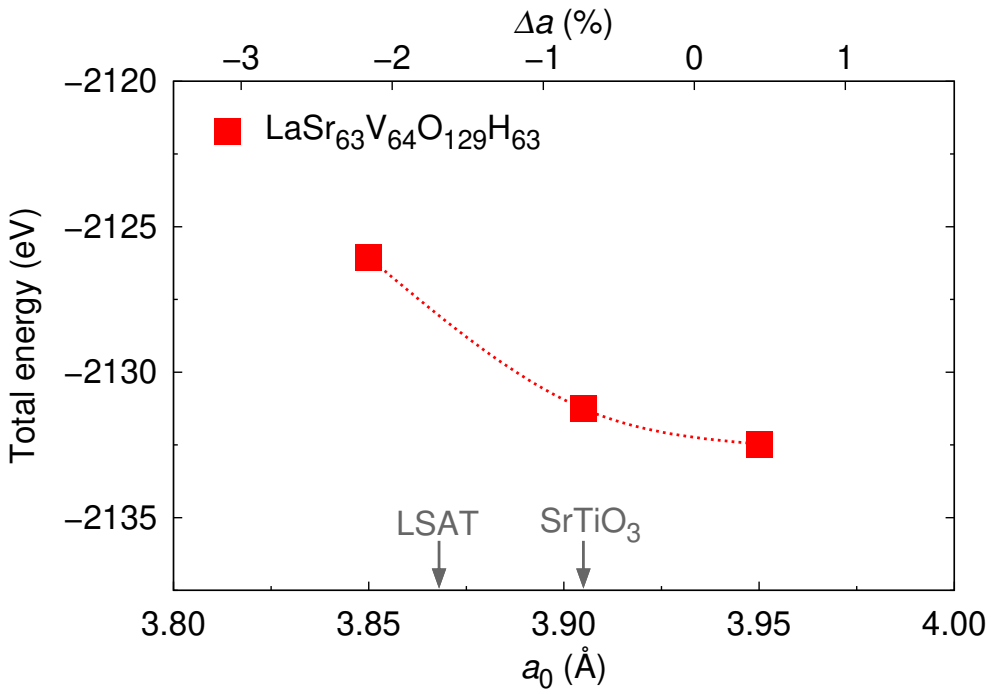

Figure S4: Calculated total energy under biaxial strain for $Sr_{1-x}La_xVO_{2+x}H_x$, where the composition with $x = 1/64$ ($\sim 1.6\%$) was examined (i.e., $LaSr_{63}V_{64}O_{129}H_{63}$). The upper axis represents the substrate strain $\Delta a (= (a_0 - a)/a_0)$, estimated from the in-plane lattice parameter a of bulk $SrVO_2H$.[S8] a_0 is the in-plane lattice parameter of the substrate.